DOI: 10.24352/UB.OVGU-2017-071

TECHNISCHE MECHANIK, 35, 2, (2015), 71– 79
submitted: June 15, 2015

# Simulation of Flow Behavior and Texture Evolution of Cu-Ag composites incorporating XRD data

Srihari Dodla, A. Bertram, M. Krüger

*This paper investigates the effect of cold drawing operations on the evolution of microstructure and texture in Cu-Ag composites. We use a crystal plasticity model to capture the flow behavior and texture of two different cold drawn composites. The three-dimension finite element simulations are able to capture the formation of Cu/Ag lamellar and grain structure inside the representative volume element (RVE). Stress-strain curves from compression tests and the measured texture after compression are presented. The numerical model is validated by experimental compression tests for a constant strain rate $10^{-2}\ s^{-1}$ at room temperature. The numerical simulations show the good capabilities of the model in reproducing the measurements.*

## 1 Introduction

Copper (Cu) shows high thermal and electrical conductivity among other engineering materials, while it has low strength in pure form. It has been shown that copper based composites can produce high mechanical strength for magnetic applications. In the literature Han et al. (1999), Cu-Ag composites have the potential to produce nano-structured composites by both casting and forming operations. Nano-structured Cu-Ag composites show a deformation induced increase of strength due to the Hall-Petch effect.
Cu-Ag composites at the crystalline level feature a face centered cubic (fcc) lattice structure. Hence, these composites have the same slip system. Furthermore, they have high stress-strain compatibility. Cu-Ag composites can be cold worked, which causes nano-size lamellar Cu and Ag filaments resulting an increase in strength of the material (e.g., Sakai et al. (1991)). Heringhaus (1998) performed compression experiments on Cu-Ag composites of various degrees of wire deformation; in their samples, the flow stress increases with an increase in wire deformation. Furthermore, the average lamella thickness decreases with increase in wire deformation. In addition, the flow behavior of the compressed samples will depend on the microstructure such as the crystallographic texture. The anisotropic flow behavior of two-phase composites is mainly due to preferred crystal orientations (Bunge (1993)). Hence the crystallographic texture analysis plays a major role when studying the macroscopic flow behavior.
Several studies of flow behavior and texture evolution of materials in metal forming have focused on single phase materials. For example, phenomelogical crystal plasticity models are mainly chosen for capturing the texture evolution in these cases by mean-field homogenization methods such as the Taylor model (Kalidindi et al. (2009), Shaffer et al. (2010)), or self-consistent schemes (Lebensohn et al. (2007)). Spectral (Eisenlohr et al. (2013); Lebensohn (2001)) and finite element (Miehe et al. (1999), Roters et al. (2010), Kalidindi et al. (1992)) methods with crystal plasticity material models have been used to study the deformation behavior considering many grain interactions. These techniques (Spectral Fast Fourier transform, FEM with a crystal plasticity material model) model the grain microstructure and the effects of grain interactions on local stress and strain fields.
In the case of two-phase composites, the presence of grain/phase boundaries will effect the crystallographic texture. Therefore it is necessary to understand and to predict the flow behavior and crystallographic texture in composites under finite deformations. Beyerlein et al. (2013, 2011) performed experiments to study the texture effects in two-phase composites such as Cu/Nb and Cu/Ag showing the importance of the layer thickness on crystallographic texture. Jia et al. (2013) studied the influence of shear banding on Cu/Nb and Cu/Ag bicrystals. Recently Hansen et al. (2013) have shown that FEM with crystal plasticity material models can successfully predict the crystallographic texture in roll-bonded Cu-Nb layers. In order to predict the complex mechanical behavior of textured Cu-Ag composites, a reliable material model is necessary to consider lamellar and grain structures at lower length scales. Studies on flow behavior and texture evolution considering grain/lamella scales in cold-drawn two-phase composites are even more limited. We point out that most of the foregoing two-phase studies have been modeled either at the grain scale or the lamella scale. However, finite element methods combining two different scales (lamella and grain) are limited. The development of finite element method with crystal plasticity material models,

presents a new challenge in modeling of two-phase lamellar composites under finite deformations.
The goal of this work is to study the flow-behavior and crystallographic texture of cold drawn Cu-Ag composites at two different drawing reductions $\eta_1 = 0.9$ and $\eta_2 = 2.1$. We show that finite element simulations with a crystal plasticity material model can successfully combine the two (lamella, grain) scales and also predict the flow behavior. Furthermore, the model is validated in the longitudinal direction by the flow curves and the crystallographic texture. The approximated texture for a small number of grains predicts well the flow behavior and crystallographic texture. From the experimental and simulation results we conclude that the texture is more pronounced after compression testing than initially.

**Notation**. We use the symbolic notation given in the continuum mechanics text book Bertram (2012). Scalars, vectors, second-order and fourth-order tensors are denoted by $a$, $\mathbf{a}$, $\mathbf{A}$, and $\mathbb{A}$, respectively. The scalar, dyadic, and Rayleigh product are given by $\cdot$, $\otimes$, and $*$, respectively, where $\mathbf{a} \cdot \mathbf{b} := a_i b_i$, $\mathbf{a} \otimes \mathbf{b} := a_i b_j \mathbf{e}_i \otimes \mathbf{e}_j$, $\mathbf{A} * \mathbb{C} := C_{ijkl} \mathbf{A}\mathbf{e}_i \otimes \mathbf{A}\mathbf{e}_j \otimes \mathbf{A}\mathbf{e}_k \otimes \mathbf{A}\mathbf{e}_l$. : denotes the double contraction between tensors, *i.e.,* $\mathbf{A} : \mathbf{B} := A_{ij} B_{ij}$. $\mathbf{A}^T$, $\mathbf{A}^{-1}$ and $\dot{\mathbf{A}}$ denote the transpose, the inverse, and the material time derivative of a second-order tensor $\mathbf{A}$. The linear mapping of a second-order tensor $\mathbf{A}$ by a fourth-order tensor $\mathbb{C}$ is written as $\mathbb{C}\,[\mathbf{A}]$.

## 2 Experiments

The Cu-Ag rods are cold drawn, which resulted in 12.4 mm and 6.7 mm diameter, respectively. Both samples exhibit a crystallographic texture with a mean grain size of 50 $\mu$m and 40 $\mu$m, respectively. The bulk texture has been measured using a X-ray diffraction method. The resulting $\{111\}$, $\{220\}$ pole figures in transverse direction of drawn samples ($\eta_1$, $\eta_2$) in Figure 1 indicate a strong texture. These pole figures of both samples have been approximated by a set of 100 discrete orientations (Figure 1) using Matlab tool box MTEX (Hielscher and Schaeben (2008), Bachmann et al. (2010a), Hielscher et al. (2010), Bachmann et al. (2010b)). Compression tests are performed on a universal testing machine at a constant strain rate of $10^{-2}$ s$^{-1}$ at room temperature. Since the crystallographic slip is isochoric and therefore the incompressibilty assumption is applied when calculating the true stresses and true strains. A detailed description of the microstructure and compression tests can be found in Dodla et al. (2015b).

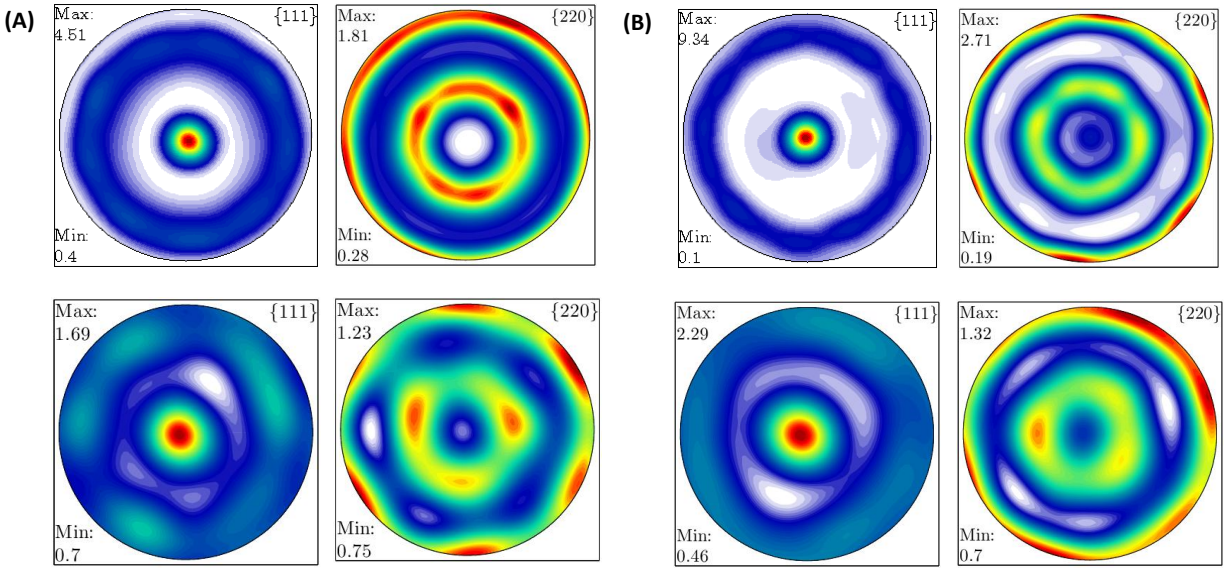


Figure 1: (A) Pole figures, measured (top) and simulated (bottom) of sample $\eta_1$, (B) Pole figures, measured (top) and simulated (bottom) of sample $\eta_2$.

## 3 Prediction and validation

### 3.1 Material model

We use an elasto-viscoplastic single crystal constitutive model in the lamellar structure of the Cu and Ag phases. The stresses are given by an anisotropic linear elastic law

$$\mathbf{T}^{2PK} = \mathbb{K}[\mathbf{E}^G] \tag{1}$$

with

$$\mathbf{E}^G = \frac{1}{2}(\mathbf{F}^T\mathbf{F} - \mathbf{I}) \tag{2}$$

where $\mathbf{T}^{2PK}$ is the 2nd Piola-Kirchhoff stress tensor, $\mathbf{E}^G$ is the Green strain tensor, $\mathbf{F}$ is the deformation gradient, and $\mathbf{I}$ is the second-order identity tensor. $\mathbb{K}$ denotes the fourth-order stiffness tetrad in the current state. In general, if the material undergoes plastic deformations, the elastic law is not constant in time because of yielding. Hence it is necessary to transform it into a time-independent constant elastic reference law

$$\tilde{\mathbf{T}}^{2PK} = \tilde{\mathbb{K}}[\tilde{\mathbf{E}}^G] \tag{3}$$

with

$$\tilde{\mathbf{E}}^G = \frac{1}{2}(\mathbf{P}^T\mathbf{F}^T\mathbf{F}\mathbf{P} - \mathbf{P}^T\mathbf{P}) \tag{4}$$

where the tensor $\mathbf{P}$ relates the variables in the undistorted placement to the reference placement. In the following equations, tilde ($\sim$) refers to all variables which are described with respect to the initially undistorted lattice base. $\tilde{\mathbb{K}}$ denotes the fourth-order constant stiffness tetrad for a cubic crystal. The tilde indicates that the $\tilde{\mathbb{K}}$ is formulated with respect to the undistorted placement. The stiffness tetrad $\mathbb{K}$ is represented by the six by six Voigt matrices and the components refer to the normalised orthonormal basis $\mathbf{B}_\alpha$ of symmetric second-order tensors (Cowin (1989); Böhlke (2001)), i.e., $K_{\alpha\beta} = \mathbf{B}_\alpha : \mathbb{K}\,[\mathbf{B}_\beta]$

$$\mathbb{K} = \begin{bmatrix} K_{11} & K_{12} & K_{12} & 0 & 0 & 0 \\ & K_{11} & K_{12} & 0 & 0 & 0 \\ & & K_{11} & 0 & 0 & 0 \\ & & & 2K_{44} & 0 & 0 \\ & sym. & & & 2K_{44} & 0 \\ & & & & & 2K_{44} \end{bmatrix} \mathbf{B}_\alpha \otimes \mathbf{B}_\beta \tag{5}$$

$$\mathbf{B}_1 = \mathbf{e}_1 \otimes \mathbf{e}_1, \mathbf{B}_2 = \mathbf{e}_2 \otimes \mathbf{e}_2, \mathbf{B}_3 = \mathbf{e}_3 \otimes \mathbf{e}_3 \tag{6}$$

$$\mathbf{B}_4 = \frac{\sqrt{2}}{2}(\mathbf{e}_2 \otimes \mathbf{e}_3 + \mathbf{e}_3 \otimes \mathbf{e}_2) \tag{7}$$

$$\mathbf{B}_5 = \frac{\sqrt{2}}{2}(\mathbf{e}_1 \otimes \mathbf{e}_3 + \mathbf{e}_3 \otimes \mathbf{e}_1) \tag{8}$$

$$\mathbf{B}_6 = \frac{\sqrt{2}}{2}(\mathbf{e}_1 \otimes \mathbf{e}_2 + \mathbf{e}_2 \otimes \mathbf{e}_1) \tag{9}$$

Copper and silver materials have a face centered cubic (fcc) crystal structure. The three independent elastic constants for copper are $K_{11} = 170$ GPa, $K_{12} = 124$ GPa and $K_{44} = 75$ GPa, and for silver $K_{11} = 123.99$ GPa, $K_{12} = 93.67$ GPa and $K_{44} = 46.12$ GPa (Kalidindi and Anand (1993), Dodla et al. (2015a)).
We used the viscous ansatz of the Hutchinson (1976) flow rule to calculate the shear-rates

$$\dot{\gamma}^\alpha = \dot{\gamma}_0 sgn(\tau^\alpha)\,|\frac{\tau^\alpha}{\tau_c(\gamma)}|^m \tag{10}$$

where $\dot{\gamma}_0$ is a constant reference shear rate, and the exponent $m$ measures the strain sensitivity of the material, and $\tau_c$ is the critical resolved shear stress, which is identical for all slip systems. The evolution of the critical resolved shear stress of all slip systems as a function of shear $\gamma$ is described by a Voce-type hardening law (Tome et al. (1984))

$$\tau_c^{\alpha}(\gamma) = \tau_{c_0} + (\tau_s + \theta_\infty \gamma)(1 - \exp(-\theta_0 \gamma / \tau_s)) \tag{11}$$

with

$$\gamma = \int \sum_{\alpha} |\dot{\gamma}_\alpha| \, \mathrm{dt} \tag{12}$$

$\gamma$ is given by the sum of shear rates of all slip systems. The Voce-type hardening rule consists of four hardening parameters, namely the initial resolved shear stress $\tau_{c_0}$, a saturation stress $\tau_s$, an initial hardening modulus $\theta_0$, and a remaining hardening modulus $\theta_\infty$. The material model has been implemented into the user subroutine (UMAT) of the finite element package ABAQUS (1990). A Newton-Raphson iteration has been applied using a backward Euler scheme (Böhlke et al. (2006)).

### 3.2 Homogenization of stresses

Prescribing the displacement gradient $\bar{\mathbf{H}}$, the stresses have been computed based on the assumption of equivalence of work on the micro and mesoscale (Hill (1963)). The $1^{st}$ Piola-Kirchhoff stresses on the local ($\mathbf{T}^{1PK}$) and the average ($\bar{\mathbf{T}}^{1PK}$) stresses are related by

$$\bar{\mathbf{T}}^{1PK} = \frac{1}{V} \int_V \mathbf{T}^{1PK} dV \tag{13}$$

The reference volume $V$ is taken as the volume average of the RVE. The Macro/meso fields are determined by homogenizing the corresponding micro fields.

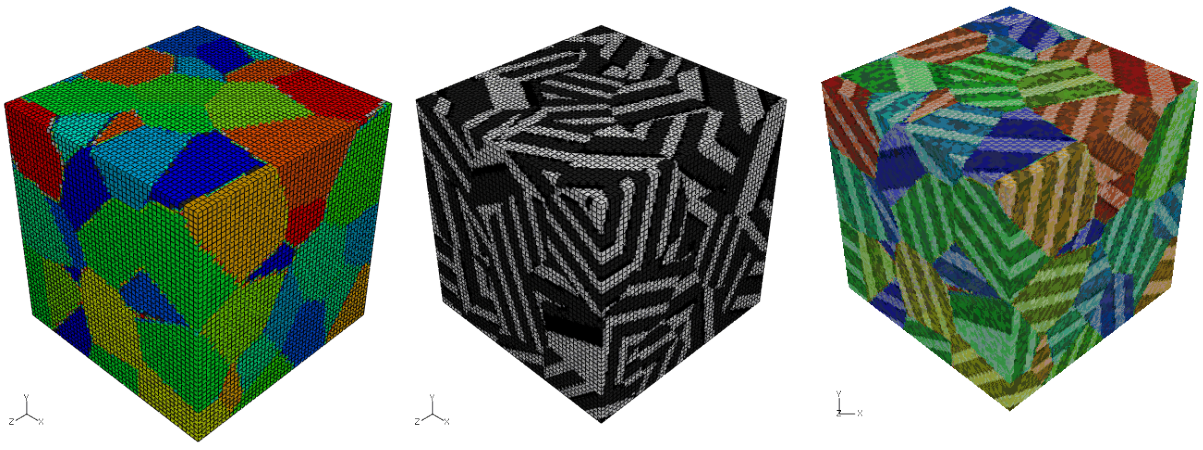

Figure 2: Three dimensional view of Voronoi microstructure (left), Cu and Ag lamellar structure inside the grains (center), and combination of both grain structure and lamellar structure of Cu, Ag phases inside the RVE (right)

### 3.3 Finite element simulations of the lamellar structure

In this section, finite element simulations of copper-silver composites with a lamellar structure are modeled using ABAQUS (1990). To predict the flow behavior of Cu-Ag polycrystals, a crystal plasticity material model is used in the finite element simulations which we apply for lamellar structures and complex grain structures. In this work, the grain microstructure is given as Voronoi tessellations in three dimensions. The Voronoi points of the grains are created by a Poisson process, so that these points are distributed uniformly (Poisson distribution). The number of grains represent the number of Voronoi points. A cube in the above created Voronoi structure is taken

as the representative volume element (RVE). For each Voronoi point, the interface normal is generated randomly, i.e., for every grain there is an interface normal vector which provides the information of the lamellar direction. The lamella thickness of each phase considered in the FE simulations is simply the volume fraction ($vf$) of the polycrystals, i.e., $vf_{Cu} = 0.37$ and $vf_{Ag} = 0.63$. The crystal orientation is assigned to the lamellar phases based on the information for a given integration point whether it belongs to the Cu phase or the Ag phase and to which grain. Fig. 2 presents the finite element with the Voronoi microstructure, the two Cu/Ag lamellae phases, and the lamellar structure along with grains respectively. The RVE mesh consists of 110,592 linear fully integrated hexahedral elements. Periodic boundary conditions have been applied in the simulations.

### 3.4 Prediction of material parameters

Since the composites are loaded under a constant strain rate $10^{-2}\ s^{-1}$ and spin, the velocity gradient tensor $\mathbf{L}$ is assumed to be constant. Hence the tensor $\mathbf{L}$ is related to the tensor $\mathbf{F}$ in the form of $\mathbf{F}(t) = exp(\mathbf{L}t)\mathbf{F}_0$. We begin with the Voce hardening parameters given in Beyerlein et al. (2011) for both the Cu and Ag phases. The material parameters for both the samples are obtained by simulating a uniaxial compression test at a constant strain rate $10^{-2}\ s^{-1}$ in transversal direction and comparing the results with the measured experimental data (see Fig. 3). $\dot{\gamma}_0$ is given as $0.01$, since the material is loaded at a constant strain rate of $10^{-2}s^{-1}$. Table 1 exhibits the identified parameters from Fig. 3. For more information about the identification scheme can be found in Dodla et al. (2015a).

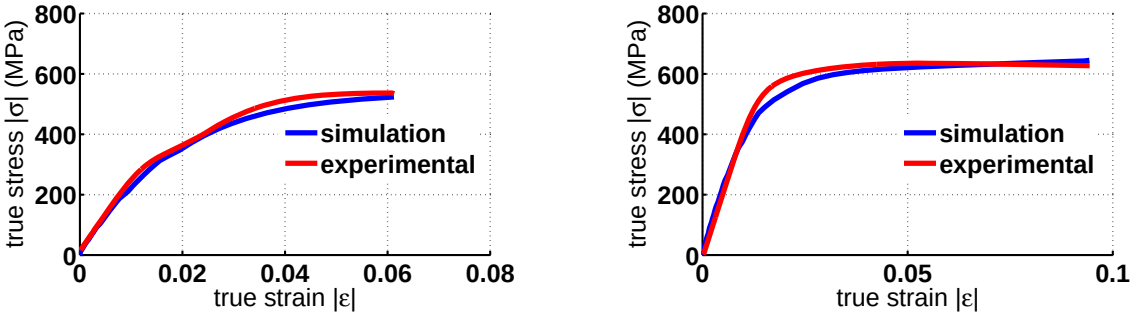


Figure 3: Predicted numerical and experimental stress-strain curves for the compression test of sample $\eta_1$ (left figure) and sample $\eta_2$ (right figure)

### 3.5 Validation results

Compression tests in the longitudinal direction have been used to validate the material model in their direction for both the samples. From these tests, the stress-strain curves can be obtained. Fig. 4 refers the comparison between the measured and simulated data of both samples ($\eta_1$, $\eta_2$). In the case of sample $\eta_1$, the numerical simulations are in good agreement with the experimental data (see Fig. 4 (left)). However, there is a slight deviation at strains below $3\%$ of the drawn sample $\eta_2$ as shown in Fig. 4 (right). This deviation may be due to the heterogeneity in the microstructure. In the experimental investigations, it is observed that the microstructure of sample $\eta_2$ shows a reduction in grain size from the center to the edge of the rod (Dodla et al. (2015b)). Moreover, the numerical simulations by only 100 grains is rather small, although sufficient to capture the main features of the real texture.

Table 1: Material parameters for Cu-Ag composites

| Material | $\dot{\gamma}_0[s^{-1}]$ | $m$ [-] | $\tau_{c_0}[MPa]$ | $\tau_s[MPa]$ | $\theta_0[MPa]$ | $\theta_\infty[MPa]$ |
|---|---|---|---|---|---|---|
| sample: $d_1$ | | | | | | |
| Cu | 0.01 | 80 | 5.5 | 227.5 | 7964 | 9.2 |
| Ag | 0.01 | 80 | 5 | 200.9 | 4501 | 20 |
| sample: $d_2$ | | | | | | |
| Cu | 0.01 | 80 | 5.5 | 241.4 | 14000 | 105 |
| Ag | 0.01 | 80 | 5 | 227.6 | 12746 | 50 |

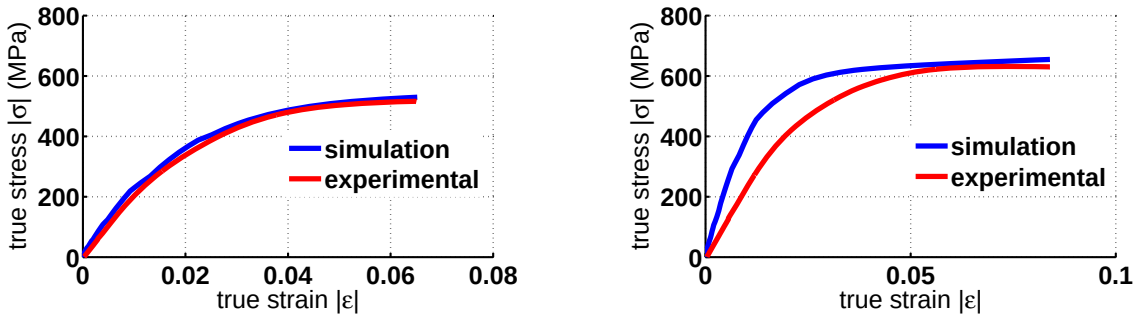


Figure 4: Measured and validated stress-strain curves for the compression test of sample $\eta_1$ (left figure) and sample $\eta_2$ (right figure)

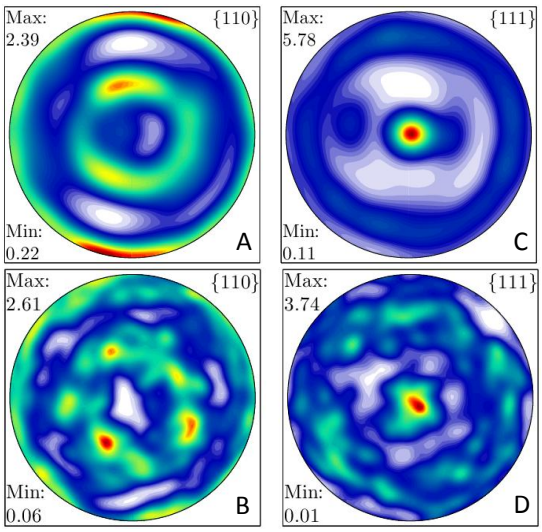


Figure 5: Pole figures $\eta_1$: (A), (C) measured and (B), (D) simulated

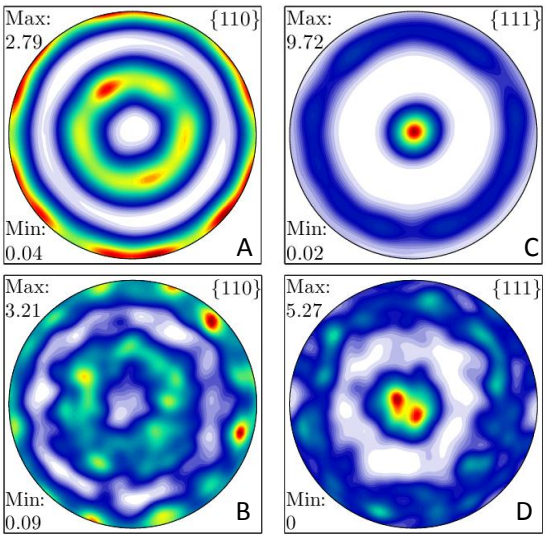


Figure 6: Pole figures $\eta_2$: (A), (C) measured and (B), (D) simulated

The measured and simulated textures in this article after compression testing are presented in terms of (110), (111) pole figures and $\phi_2(= 45°)$ section of the orientation distribution function (ODF) in the space of Euler angles $(\phi_1, \varphi) \leq 90°$. The anisotropic behavior of both samples is observable in the texture results, as shown in Fig. 5, 6, 7. The texture analysis in the ODF shows the maxima at $\{11\bar{2}\}\langle 111\rangle$ in both samples $\eta_1$ and $\eta_2$. By increase the drawing strain from sample $\eta_1$ to $\eta_2$, the maximum texture component increases from 6.72 to 12.32. Hence with increase in the drawing strain, the texture becomes stronger and more pronounced. A good agreement between the experiment and numerical simulations is observed. The finite element simulations with the approximated 100 discrete orientations of both the samples capture the above mentioned experimental observations of the crystallographic texture. However, the simulated texture is overpredicted in both the samples. The reason for this is that the number of orientations is rather small to represent the complete texture.

## 4 Summary and conclusions

Finite element simulations have been applied to study the flow behavior in two different textured samples. In particular, the combination of three different scales (lamella, grain and macro scale) as well as the incorporation of experimentally measured textures are explored. Furthermore, simulations of the flow behavior of two Cu-Ag composites have been validated by the experimentally measured stress-strain behavior and texture. The simulations have been performed by the finite element software ABAQUS. Within the lamellar structure of the Cu and Ag phases an elasto-viscoplastic single crystal constitutive model has been applied. The RVE with periodic boundary conditions is constructed as a Voronoi microstructure. In the FE simulation, compression test simulations have been performed in the longitudinal direction to validate the material parameters of the two Cu-Ag composites. From the investigations of the flow behavior, the initial texture, and the final texture after compression testing, we draw the following conclusions from the experimental and numerical results.

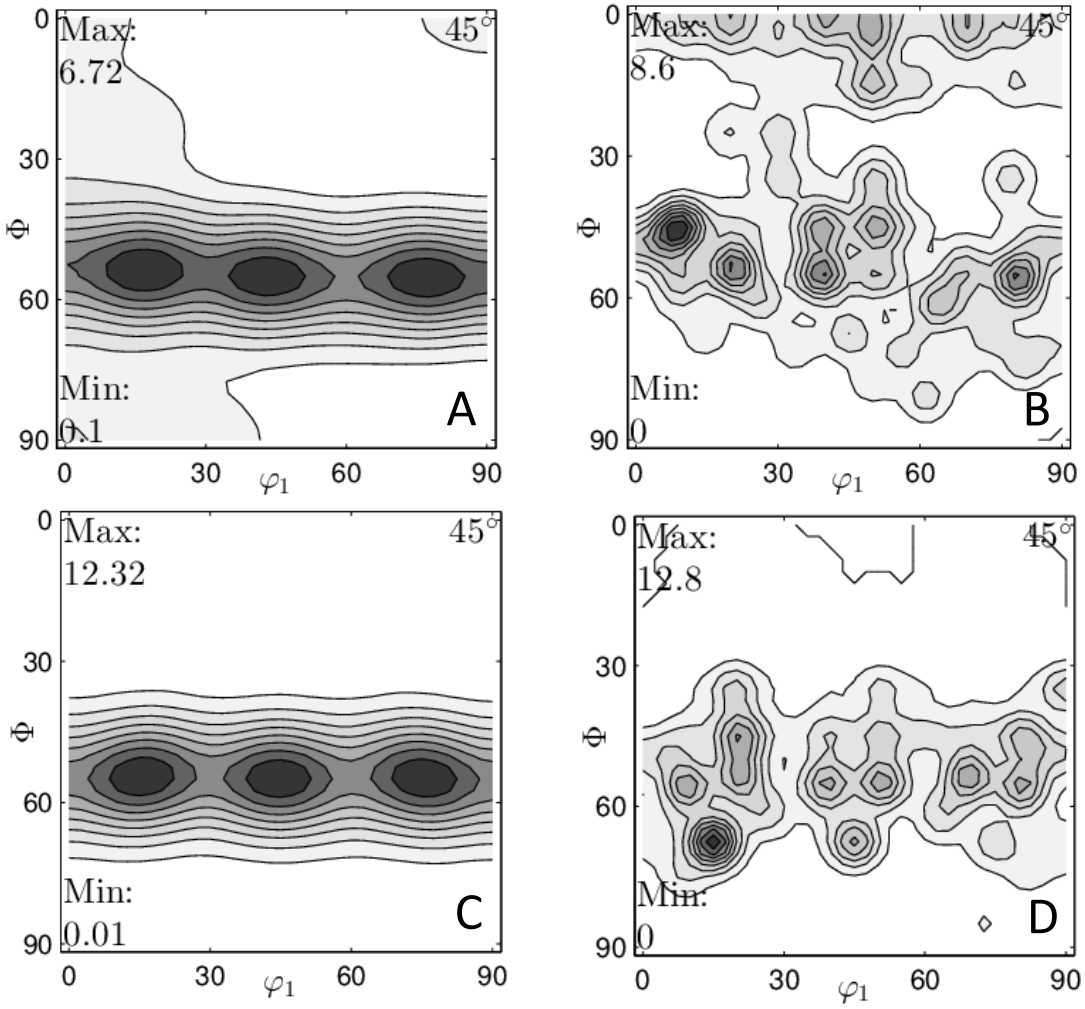


Figure 7: ODF for the drawn samples at $\varphi_2 = 45^\circ$ (A), (B) measured and simulated $\eta_1$ and (C), (D) measured and simulated $\eta_2$.

1. The flow behavior is well captured for both Cu-Ag composites, and the parameters for both composites using the elasto-viscoplastic single crystal constitutive model have been identified (see Fig. 3 (left) and 3 (right)).

2. The compressive flow behavior of the first polycrystal is validated by the numerical model approximated by an initial texture with 100 grains (see Fig. 4 (left)). In the case of the second polycrystal, the comparison of the simulated stress-strain behavior with the measured stress-strain curve shows a small deviation at strains $< 3\%$. However, the curve is in good accordance with the experimental curve at strains above $3\%$ (see Fig. 4 (right)).

3. The simulated texture of both Cu-Ag composites reproduce the experimentally observed texture. Figure 5, 6, and 7 reveals the simulated and measured textures for both samples. The simulated textures overpredict the measured textures, but the maximum texture component ($\left\{11\bar{2}\right\}\langle 111\rangle$) is well captured.

## 5 Acknowledgements

The financial support provided by the German Science Foundation (DFG) through GRK 1554 is acknowledged. We sincerely thank Thorsten Halle (Otto-von-Guericke University Magdeburg) for fruitful discussions. We thank A. Hilbig and P. Thiem for performing the XRD measurements.

## References

ABAQUS: *Reference Manuals, Hibbitt, Karlsson and Sorensen*. Addison-Wesley, Inc., Providence, RI (1990).

Bachmann, F.; Hielscher, R.; Jupp, P. E.; Pantleon, W.; Schaeben, H.; Wegert, E.: Inferential statistics of electron backscatter diffraction data from within individual crystalline grains. *Journal of Applied Crystallography*, 43, 6, (2010a), 1338–1355.

Bachmann, F.; Hielscher, R.; Schaeben, H.: Texture analysis with MTEX–Free and Open Source Software Toolbox. *Solid State Phenomena*, 160, (2010b), 63–68.

Bertram, A.: *Elasticity and Plasticity of Large Deformations - an Introduction, Third Edition*. Springer Verlag, Berlin (2012).

Beyerlein, I. J.; Mara, N. A.; Bhattacharyya, D.; Alexander, D. J.; Necker, C. T.: Texture evolution via combined slip and deformation twinning in rolled silver-copper cast eutectic nanocomposite. *Acta Materialia*, 27, (2011), 121–146.

Beyerlein, I. J.; Mara, N. A.; Carpenter, J. S.; Nizolek, T.; Mook, W. M.; Wynn, T. A.; McCabe, R. J.; Mayeur, J. R.; Kang, K.; Zheng, S.; Wang, J.; Pollock, T. M.: Interface-driven microstructure development and ultra high strength of bulk nanostructured Cu-Nb multilayers fabricated by severe plastic deformation. *J. Mater. Res.*, 28, (2013), 1799–1812.

Böhlke, T.: *Crystallographic Texture Evolution and Elastic Anisotropy: Simulation, Modeling and Applications*. Shaker Verlag, Aachen (2001).

Böhlke, T.; Risy, G.; Bertram, A.: Finite element simulation of metal forming operations with texture based material models. *Modelling and Simulation in Material Science and Engineering*, 14, (2006), 365–387.

Bunge, H.: *Texture Analysis in Materials Science*. Curvillier Verlag, Göttingen (1993).

Cowin, S.: Properties of the anisotropic elasticity tensor. *Quarterly J. of Mechanics & Appl. Maths*, 42, (1989), 249–266.

Dodla, S.; Bertram, A.; Krüger, M.: Finite element simulation of lamellar copper-silver composites. *Computational Materials Science*, 101, (2015a), 29–38.

Dodla, S.; Thiem, P.; Krüger, M.; Dietrich, D.; Bertram, A.: Investigations of microstructure and texture of Copper-Silver composites. *Journal of Alloys and Compounds*, 647, (2015b), 519–527.

Eisenlohr, P.; Diehl, M.; Lebensohn, R. A.; Roters, F.: A spectral method solution to crystal elasto-viscoplasticity at finite strains. *International Journal of Plasticity*, 46, (2013), 37–53.

Han, K.; Embury, J. D.; Sims, J. R.; Campbell, L. J.; Schneider Muntau, H. J.; Pantsyrnyi, V. I.; Shikov, A.; Nikulin, A.; Vorobieva, A.: The fabrication, properties and microstructure of Cu-Ag and Cu-Nb composite conductors. *Materials Science and Engineering A*, 267, (1999), 99–114.

Hansen, B. L.; Carpenter, J. S.; Sintay, S. D.; Bronkhorst, C. A.; McCabe, R. J.; Mayeur, J. R.; Mourad, H. M.; Beyerlein, I. J.; Mara, N. A.; Chen, S. R.; Gray Iii, G. T.: Modeling the texture evolution of Cu/Nb layered composites during rolling. *International Journal of Plasticity*, 49, (2013), 71–84.

Heringhaus, F.: *Quantitative Analysis of the Influence of th Microstructure on Strength, Resistivity, and Magnetoresistance of Eutectic Silver-Copper*. Shaker Verlag, Berlin (1998).

Hielscher, R.; Schaeben, H.: A novel pole figure inversion method: specification of the *MTEX* algorithm. *Journal of Applied Crystallography*, 41, 6, (2008), 1024–1037.

Hielscher, R.; Schaeben, H.; Siemes, H.: Orientation distribution within a single hematite crystal. *Mathematical Geosciences*, 42, (2010), 359–375.

Hill, R.: Elastic properties of reinforced solids: Some theoretical principles. *Journal of the Mechanics and Physics of Solids*, 11, (1963), 357–372.

Hutchinson, J.: Bounds and self-consistent estimates for creep of polycrystalline materials. *Proc. R. Soc. London*, A 348, (1976), 101–127.

Jia, N.; Roters, F.; Eisenlohr, P.; Raabe, D.; Zhao, X.: Simulation of shear banding in heterophase co-deformation: Example of plane strain compressed Cu-Ag and Cu-Nb metal matrix composites. *Acta Materialia*, 61, (2013), 4591–4606.

Kalidindi, S. R.; Anand, L.: Large deformation simple compression of a copper single crystal. *Metallurgical Transactions A*, 24A, (1993), 989–992.

Kalidindi, S. R.; Bronkhorst, C. A.; Anand, L.: Crystallographic texture evolution in bulk deformation processing of fcc metals. *J. Mech. Phys. Solids*, 40, (1992), 537–569.

Kalidindi, S. R.; Knezevic, M.; Niezgoda, S. J., S.: Representation of the orientation distribution function and computation of first-order elastic properties closures using discrete Fourier transforms. *Acta Mater.*, 57, (2009), 3916–3923.

Lebensohn, R.: N-site modeling of a 3D viscoplastic polycrystal using Fast Fourier Transform. *Acta Mater.*, 49, (2001), 2723–2737.

Lebensohn, R. A.; Tome, C. N.; Castaneda, P. P.: Self-consistent modelling of the mechanical behaviour of viscoplastic polycrystals incorporating intragranular field fluctuations. *Philos. Mag.*, 87, (2007), 4287–4322.

Miehe, C.; Schröder, J.; Schotte, J.: Computational homogenization analysis in finite plasticity simulation of texture development in polycrystalline materials. *Computer Methods in Applied Mechanics and Engineering*, 171, (1999), 387–418.

Roters, F.; Eisenlohr, P.; Hantcherli, L.; Tjahjanto, D. D.; Bieler, R. D., T. R.: Overview of constitutive laws, kinematics, homogenization and multiscale methods in crystal plasticity finite-element modeling: Theory, experiments, applications. *Acta Materialia*, 58, (2010), 1152–1211.

Sakai, Y.; Asano, T.; Inoue, K.; Wada, H.; Maeda, H.: Development of high strength, high conductivity Cu-Ag alloys for high field pulsed magnet use. *Applied Physics Letters*, 59, (1991), 2965–2967.

Shaffer, J. B.; Knezevic, M.; Kalidindi, S. R.: Buliding texture evolution networks for deformation processing of polycrystalline fcc metals using spectral approaches: applications to process design for targeted performance. *Int. J. Plast.*, 26, (2010), 1183–1194.

Tome, C. N.; Canova, G. R.; Kocks, U. F.; Christodoulou, N.; Jonas, J. J.: The relation between macroscopic and microscopic strain hardening in fcc polycrystals. *Acta Metallurgica 32*, pages 1637–1653.

---

*Address:* Srihari Dodla, A. Bertram, M. Krüger ,
Otto-von-Guericke-Universität Magdeburg, D-39106, Magdeburg Germany Tel. +49 391 67 52246; Fax +49 391 67 2863
email: albrecht.bertram@ovgu.de